Conclusions

Despite the quite simple design concept, the elastic wind-tunnel model is shown to be well suited for low-speed aeroelastic investigations. Furthermore, the segmented concept enables the possibility to replace individual wing sections. For example, new wing sections including control surfaces can easily be used for studies regarding control surface efficiency and aeroservoelastic response. Moreover, it is possible to design various internal wing beams with different stiffness properties for experimental comparison of aeroelastic performance on a model level. Also, new masses can be added to the individual wing sections to modify the dynamic behavior of the model.

When the experimental procedure, including both model manufacturing and wind-tunnel testing is considered, the study shows that the use of a relatively simple model concept can be very useful to provide experimental information at an early stage of a new project. The efficiency of the experimental testing is further increased as the experimental setup including load and deformation measurements as well as wind-tunnel operation can be handled by a single operator. Especially, the use of the optical positioning system in combination with passive reflecting markers for deformation measurements is shown to be very efficient.

Finally, the development of the BWB concept provides many new challenges. However, the results from this study indicate that standard numerical tools are capable of predicting the low-speed aeroelastic behavior of the BWB planform with reasonable accuracy.

Acknowledgments

This work was financially supported by the Commission of the European Union. The investigation was carried out within the project Multi-Disciplinary Design and Optimisation for Blended Wing Body Configuration, Contract G4RD-CT1999-0172.

References

[1]Sensburg, O., Schweiger, J., Tischler, V. A., and Venkayya, V. B., "Aeroelastic Tailoring of Aerodynamic Surfaces and Low Cost Wind Tunnel Model Design," *Proceedings of the International Workshop on Multidisciplinary Design Optimization*, Rept. ADA 389797, Pretoria, South Africa, 2000, pp. 240–253.

[2]Schneider, G., Hoenlinger, H., Guldner, W., and Manser, R., "Aeroelastic Tailoring Validation by Windtunnel Model Testing," *Proceedings of the European Forum on Aeroelasticity and Structural Dynamics*, Deutsche Gesellschaft Fuer Luft- und Raumfahrt, Bonn, Germany, 1989, pp. 399–408.

[3]Baker, M. L., Mendoza, R., and Hartwich, P. M., "Transonic Aeroelastic Analysis of a High Speed Transport Wind-Tunnel Model," AIAA Paper 99-1217, April 1999.

[4]French, M., and Eastep, F. E., "Aeroelastic Model Design Using Parameter Identification," *Journal of Aircraft*, Vol. 33, No. 1, 1996, pp. 198–202.

[5]Amiryants, G. A., and Ishmuratov, F. Z., "Multi-Purpose Modular Aerodynamic/Aeroelastic Model," *Proceedings of the CEAS/AIAA/AIAE International Forum on Aeroelasticity and Structural Dynamics*, Madrid, Spain, Vol. 3, June 2001, pp. 509–518.

[6]Burner, A. W., and Liu, T., "Videogrammetric Model Deformation Measurement Technique," *Journal of Aircraft*, Vol. 38, No. 4, 2001, pp. 745–754.

[7]Roman, D., Allen, J. B., and Liebeck, R. H., "Aerodynamic Design Challenges of the Blended-Wing–Body Subsonic Transport," AIAA Paper 2000-4335, Aug. 2000.

[8]Liebeck, R. H., Page, M. A., and Rawdon, B. K., "Blended-Wing–Body Subsonic Commercial Transport," AIAA Paper 98-0438, Jan. 1998.

[9]Barlow, J. B., Rae, W. H., and Pope, A., *Low-Speed Wind Tunnel Testing*, 3rd ed., Wiley, New York, 1999, pp. 683–691.

[10]Milholen, W. E., II, and Chokani, N., "Development of Semispan Model Test Techniques," *Journal of Aircraft*, Vol. 33, No. 6, 1996, pp. 1115–1122.

[11]Carlsson, M., "Aeroelastic Testing of a Sectioned Wind Tunnel Model," Dept. of Aeronautics, Rept. C2000-06, Royal Inst. of Technology, Stockholm, June 2000.

[12]Rodden, W. P., and Johnson, E. H., "MSC/NASTRAN Aeroelastic Analysis Users Guide," Ver. 68, MacNeal–Schwendler, Los Angeles, Oct. 1994.

[13]Albano, E., and Rodden, W. P., "A Doublet-Lattice Method for Calculating Lift Distributions on Oscillating Surfaces in Subsonic Flows," *AIAA Journal*, Vol. 7, No. 2, 1969, pp. 279–285.

[14]Qualisys, A. B., "ProReflex," Ver. 6.41, Technical Reference, Sävedalen, Sweden, 1997.

[15]Kuttenkeuler, J., and Carlsson, M., "Optical Deformation Measurements in Wind Tunnel Testing," *Proceedings of the CEAS/AIAA/AIAE International Forum on Aeroelasticity and Structural Dynamics*, Madrid, Spain, Vol. 3, June 2001, pp. 499–508.

Mixed Jameson/Total-Variation-Diminishing Scheme Applied to Simulating Rotor Airfoil Flowfield

Yihua Cao,* Jifei Wang,† and Yuan Su‡
Beijing University of Aeronautics and Astronautics, Beijing 100083, People's Republic of China

Introduction

WITH the rapid development of computational technology, numerical simulation by solving classical governing equations of fluid dynamics is playing a more and more important role in air vehicle aerodynamics, specifically in rotorcraft aerodynamics (Ref. 1). To date, various computational methods have been investigated, and the finite volume central differential scheme created by Jameson et al.[2] has been demonstrated to be a robust method and has been widely used in computational rotor aerodynamics. More recently, many high-resolution schemes are emerging, for example, the total-variation-diminishing (TVD) scheme[3,4] is a representative one.

In this Note, a classical rotor airfoil (NACA0012) has been chosen as the example to demonstrate the flexibility of a mixed Jameson/TVD scheme in computational rotor aerodynamics. At first, Jameson's finite volume central differential scheme is implemented to solve the Euler equations describing the flowfield around the airfoil just mentioned. Then, a mixed Jameson/TVD scheme is constructed by correcting artificial viscous terms to capture the position of the shock wave more precisely. Also, for the first time this scheme is used to solve the Euler equations for the simulation of the flowfield around a rotor airfoil. Additionally, with regard to the Euler equations' deficiency in reflecting viscous effects, Jameson's scheme is applied to solve the turbulent Navier–Stokes (N–S) equations, which is a good start for further numerical calculation of helicopter rotor drag force and power.

Governing Equations

For two-dimensional problems the compressible N–S equations can be represented in the following conservation form:

$$\frac{\partial W}{\partial t}+\frac{\partial F}{\partial x}+\frac{\partial G}{\partial y}=\frac{\partial R}{\partial x}+\frac{\partial S}{\partial y} \tag{1}$$

where

$$W=\begin{bmatrix}\rho\\ \rho u\\ \rho v\\ \rho e\end{bmatrix}\quad F=\begin{bmatrix}\rho u\\ \rho u^2+p\\ \rho uv\\ \rho uh\end{bmatrix}\quad G=\begin{bmatrix}\rho v\\ \rho uv\\ \rho v^2+p\\ \rho vh\end{bmatrix}$$

Received 31 May 2002; revision received 22 September 2002; accepted for publication 27 September 2002.

*Professor, Department of Flight Vehicle Design and Applied Mechanics.
†Doctor, Department of Flight Vehicle Design and Applied Mechanics.
‡Lecturer, Department of Flight Vehicle Design and Applied Mechanics.

$$R = \begin{bmatrix} 0 \\ \tau_{xx} \\ \tau_{yx} \\ \kappa T_x + \tau_{xx}u + \tau_{yx}v \end{bmatrix}, \quad S = \begin{bmatrix} 0 \\ \tau_{xy} \\ \tau_{yy} \\ \kappa T_y + \tau_{xy}u + \tau_{yy}v \end{bmatrix} \tag{2}$$

$$\tau_{xx} = 2\mu\frac{\partial u}{\partial x} + \lambda\left(\frac{\partial u}{\partial x} + \frac{\partial v}{\partial y}\right), \qquad \tau_{xy} = \tau_{yx} = \mu\left(\frac{\partial u}{\partial y} + \frac{\partial v}{\partial x}\right)$$

$$\tau_{yy} = 2\mu\frac{\partial v}{\partial y} + \lambda\left(\frac{\partial u}{\partial x} + \frac{\partial v}{\partial y}\right), \qquad \lambda = -\frac{2}{3}\mu \tag{3}$$

In Eq. (1), R and S are viscous terms. If nonviscous assumptions are applied, then R and S, both equal to zero, and the N–S equations regress into the Euler equation. Also, μ represents the viscous coefficient, and κ is the heat conductive coefficient. In turbulent flow their relationship is given by

$$\mu = \mu_t + \mu_l, \qquad \kappa = c_p(\mu_l/p_{\mathrm{rl}} + \mu_t/p_{\mathrm{rt}}) \tag{4}$$

where μ_t and μ_l represent turbulent and laminar viscous coefficients. The μ_l can be obtained from the Sutherland formula,[5] whereas μ_t, being subject to a different turbulence model, is calculated using the Baldwin–Lomax algebraic model,[6] in which p_{rl} is 0.72 and p_{rt} is 0.9.

In the expressions for W, F and G, e and h are unit energy and unit enthalpy, respectively. For the solution of those equations, other equations should be employed as follows:

$$e = p/(\gamma - 1)\rho + \tfrac{1}{2}(u^2 + v^2)$$

$$h = e + p/\rho, \qquad p = \rho RT \tag{5}$$

Numerical Method

Numerical Approximation

If we define a unit vector (e_x, e_y) in Cartesian coordinates and implement the finite volume method, then Eq. (1) can be revised into integral form:

$$\frac{\partial}{\partial t}\iint_{\Omega} W\,\mathrm{d}x\,\mathrm{d}y + \int_{\partial\Omega} \bar{\bar{H}}\cdot\boldsymbol{n}\,\mathrm{d}s = \int \bar{\bar{H}}_v\cdot\boldsymbol{n}\,\mathrm{d}s \tag{6}$$

where $\partial\Omega$ represents the boundary curve of a unit cell Ω and $\boldsymbol{n}$ is the unit normal vector of $\mathrm{d}s$. The second-order tensor $\bar{\bar{H}}$ and $\bar{\bar{H}}_v$ can be defined as

$$\bar{\bar{H}} = F\boldsymbol{e}_x + G\boldsymbol{e}_y \tag{7}$$

$$\bar{\bar{H}}_v = R\boldsymbol{e}_x + S\boldsymbol{e}_y \tag{8}$$

If all physical parameters at the center of each unit cell are known, then Eq. (6) can be further approximated for each unit cell in the computational domain so that the following ordinary differential equation can be obtained:

$$\frac{\mathrm{d}}{\mathrm{d}t}(V_{i,j}W_{i,j}) + P_{i,j} - P_{vi,j} = 0 \tag{9}$$

$$p_{i,j} = (\bar{\bar{H}}\cdot\boldsymbol{S})_{i+\frac{1}{2},j} + (\bar{\bar{H}}\cdot\boldsymbol{S})_{i,j+\frac{1}{2}} - (\bar{\bar{H}}\cdot\boldsymbol{S})_{i-\frac{1}{2},j} - (\bar{\bar{H}}\cdot\boldsymbol{S})_{i,j-\frac{1}{2}}$$

$$p_{vi,j} = (\bar{\bar{H}}_v\cdot\boldsymbol{S})_{i+\frac{1}{2},j} + (\bar{\bar{H}}_v\cdot\boldsymbol{S})_{i,j+\frac{1}{2}} - (\bar{\bar{H}}_v\cdot\boldsymbol{S})_{i-\frac{1}{2},j} - (\bar{\bar{H}}_v\cdot\boldsymbol{S})_{i,j-\frac{1}{2}}$$

where $V_{i,j}$ represents the area of the unit cell, $P_{i,j}$ the net flux, and $P_{vi,j}$ the net viscous flux. When the Euler equation is solved, $P_{vi,j}$ is zero. As for the N–S equation, if the Reynolds number of the flowfield is high enough then the thin layer assumption is applicable, that is,

$$p_{vi,j} = (\bar{\bar{H}}_v\cdot\boldsymbol{S})_{i,j+\frac{1}{2}} - (\bar{\bar{H}}_v\cdot\boldsymbol{S})_{i,j-\frac{1}{2}}$$

Artificial Viscous Term

As the central differential scheme is not dissipative, in order to restrain numerical oscillations and damp computational error and also ensure convergence an artificial viscous term is necessary. Equation (9) can be revised as

$$\frac{\mathrm{d}}{\mathrm{d}t}(V_{i,j}W_{i,j}) + P_{i,j} - P_{vi,j} - D_{i,j} = 0 \tag{10}$$

$$D_{i,j} = d_{i+\frac{1}{2},j} - d_{i-\frac{1}{2},j} + d_{i,j+\frac{1}{2}} - d_{i,j-\frac{1}{2}} \tag{11}$$

where $D_{i,j}$ is the artificial viscous term, which is an important factor in different computational schemes. The well-known self-adaptive terms created by Jameson et al.[2] consist of a second-order and a fourth-order term of W plus a self-adaptive switch term. Where the gradient is large, the second-order term dominates the fourth-order term, and where the gradient is small the fourth-order term dominates. Through such mechanisms the shock wave can be automatically captured and numerical oscillations near the shock wave minimized.

Based on the TVD dissipation term presented in Yee et al.[3] and Wang and Widhopf,[4] we construct a new Jameson/TVD mixed artificial viscous term using a flux-correction method, that is,

$$d_{i+\frac{1}{2},j} = \sum_{l=1}^{4} \beta^l_{i+\frac{1}{2},j} R^l_{i+\frac{1}{2},j} \tag{11a}$$

$$\beta^l_{i+\frac{1}{2}} = Q^l\left(v^l_{i+\frac{1}{2}} + r^l_{i+\frac{1}{2}}\right)\alpha^l_{i+\frac{1}{2}} - \left(g^l_i + g^l_{i+1}\right) \tag{11b}$$

$$R_{i+\frac{1}{2}} = \begin{bmatrix} 1 & 1 & 1 & 0 \\ \hat{u}_{i+\frac{1}{2}} - \hat{c}_{i+\frac{1}{2}} & \hat{u}_{i+\frac{1}{2}} & \hat{u}_{i+\frac{1}{2}} + \hat{c}_{i+\frac{1}{2}} & 0 \\ \hat{v}_{i+\frac{1}{2}} & \hat{v}_{i+\frac{1}{2}} & \hat{v}_{i+\frac{1}{2}} & 1 \\ \hat{H}_{i+\frac{1}{2}} - \hat{u}_{i+\frac{1}{2}}\hat{c}_{i+\frac{1}{2}} & \left(\hat{u}^2_{i+\frac{1}{2}} + \hat{v}^2_{i+\frac{1}{2}}\right)/2 & \hat{H}_{i+\frac{1}{2}} + \hat{u}_{i+\frac{1}{2}}\hat{c}_{i+\frac{1}{2}} & \hat{v}_{i+\frac{1}{2}} \end{bmatrix} \tag{11c}$$

where

$$v^l_{i+\frac{1}{2}} = \lambda_i a^l_{i+\frac{1}{2}}, \qquad a^1_{i+\frac{1}{2}} = \hat{u}_{i+\frac{1}{2}} - \hat{c}_{i+\frac{1}{2}}, \qquad a^2_{i+\frac{1}{2}} = \hat{u}_{i+\frac{1}{2}}$$

$$a^3_{i+\frac{1}{2}} = \hat{u}_{i+\frac{1}{2}} + \hat{c}_{i+\frac{1}{2}}, \qquad a^4_{i+\frac{1}{2}} = \hat{u}_{i+\frac{1}{2}}$$

$$\hat{u}_{i+\frac{1}{2}} = \left\langle \rho^{\frac{1}{2}}u\right\rangle \Big/ \left\langle \rho^{\frac{1}{2}}\right\rangle, \qquad \hat{c}_{i+\frac{1}{2}} = \left\{(\gamma-1)\left(\hat{H}_{i+\frac{1}{2}} - \tfrac{1}{2}\hat{u}^2_{i+\frac{1}{2}}\right)\right\}^{\frac{1}{2}}$$

$$\langle b\rangle = \tfrac{1}{2}(b_i + b_{i-1}), \qquad H = \gamma p/(\gamma-1)\rho + \tfrac{1}{2}(u^2+v^2)$$

$$Q(x) = \tfrac{1}{2}(x^2/\varepsilon + \varepsilon), \qquad \alpha^1_{i+\frac{1}{2}} = \tfrac{1}{2}(C_1 - C_2)$$

$$\alpha^2_{i+\frac{1}{2}} = [\rho]_{i+\frac{1}{2}} - C_1, \qquad \alpha^3_{i+\frac{1}{2}} = \tfrac{1}{2}(C_1 + C_2)$$

$$\alpha^4_{i+\frac{1}{2}} = [\rho v]_{i+\frac{1}{2}} - \hat{v}_{i+\frac{1}{2}}[\rho]_{i+\frac{1}{2}}$$

$$C_1 = (\gamma-1)\left\{[\rho e]_{i+\frac{1}{2}} + \tfrac{1}{2}\left(\hat{u}^2_{i+\frac{1}{2}} - \hat{v}^2_{i+\frac{1}{2}}\right)[\rho]_{i+\frac{1}{2}} - \hat{u}_{i+\frac{1}{2}}[\rho u]_{i+\frac{1}{2}} - \hat{v}_{i+\frac{1}{2}}[\rho v]_{i+\frac{1}{2}}\right\} \Big/ \hat{c}^2_{i+\frac{1}{2}}$$

$$C_2 = \left\{[\rho u]_{i+\frac{1}{2}} - \hat{u}_{i+\frac{1}{2}}[\rho]_{i+\frac{1}{2}}\right\}\Big/\hat{c}_{i+\frac{1}{2}}, \qquad g_i^1 = \bar{g}_i^1 + \theta_i \bar{\bar{g}}_i^1$$

$$\bar{g}_i^l = s_{i+\frac{1}{2}}^l \max\left[0, \min\left(\left|\tilde{g}_{i+\frac{1}{2}}^l\right|, \tilde{g}_{i-\frac{1}{2}}^l s_{i+\frac{1}{2}}^l\right)\right]$$

$$\tilde{g}_{i+\frac{1}{2}}^l = \frac{1}{2}\left[Q^l\left(v_{i+\frac{1}{2}}^l\right) - \left(v_{i+\frac{1}{2}}^l\right)^2\right]\alpha_{i+\frac{1}{2}}^l, \qquad s_{i+\frac{1}{2}}^l = \mathrm{sgn}\left(\tilde{g}_{i+\frac{1}{2}}^l\right)$$

$$\gamma_{i+\frac{1}{2}}^l = \left(\bar{g}_{i+1}^l - \bar{g}_i^l\right)\Big/\alpha_{i+\frac{1}{2}}^l \qquad \text{when} \qquad \alpha_{i+\frac{1}{2}}^l \neq 0$$

$$= 0 \qquad \text{when} \qquad \alpha_{i+\frac{1}{2}}^l = 0$$

$$\bar{\bar{g}}_i^l = s \max\left[0, \min\left(s\sigma_{i-\frac{1}{2}}\alpha_{i-\frac{1}{2}}, \sigma_{i+\frac{1}{2}}\left|\alpha_{i=\frac{1}{2}}\right|\right)\right]$$

$$s = \mathrm{sgn}\left(\alpha_{i+\frac{1}{2}}\right), \qquad \sigma_{i+\frac{1}{2}} = \frac{1}{2}\left[1 - Q\left(v_{i+\frac{1}{2}}\right)\right]$$

$$\theta_i = 0.25\bar{\theta}_i + 0.75\bar{\theta}_i^{1.5}$$

$$\bar{\theta}_i = \left|\alpha_{i+\frac{1}{2}} - \alpha_{i-\frac{1}{2}}\right|\Big/\left(\left|\alpha_{i+\frac{1}{2}}\right| + \left|\alpha_{i-\frac{1}{2}}\right|\right)$$

Time-Stepping Advance

With subscripts omitted, Eq. (10) can be revised as

$$\frac{\mathrm{d}W}{\mathrm{d}t} + R(W) = 0 \tag{12}$$

where

$$R(W) = (1/V_{i,j})(P_{i,j} - P_{vi,j} - D_{i,j}) \tag{13}$$

Equation (12) can be solved using a multistep Runge–Kutta method, that is,

$$W^{(0)} = W^n, \qquad W^{(1)} = W^{(0)} - \alpha_1 \Delta t R\left(W^{(0)}\right)$$

$$W^{(2)} = W^{(0)} - \alpha_2 \Delta t R\left(W^{(1)}\right), \qquad W^{(3)} = W^{(0)} - a_3 \Delta t R\left(W^{(2)}\right)$$

$$W^{(4)} = W^{(0)} - \alpha_4 \Delta t R\left(W^{(3)}\right), \qquad W^{n+1} = W^{(4)} \tag{14}$$

In practice, the physical viscous term and artificial viscous term are calculated only at the first iteration step so as to alleviate computation cost.

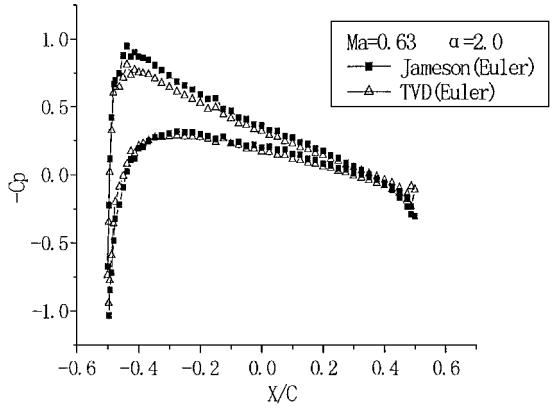

Fig. 1 Distribution of surface-pressure coefficient.

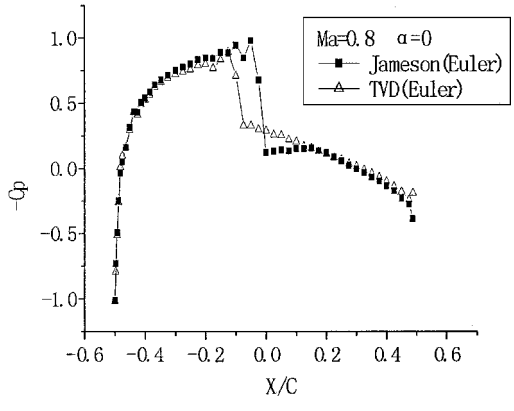

Fig. 2 Distribution of surface-pressure coefficient.

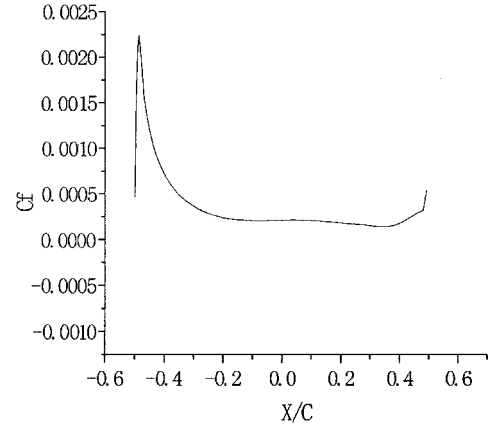

Fig. 3 Distribution of surface-friction coefficient.

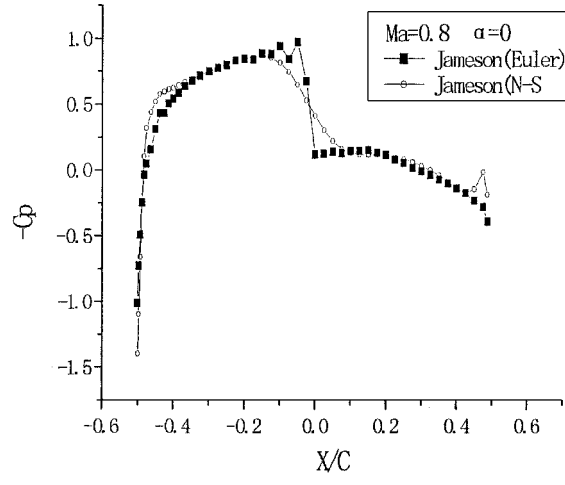

Fig. 4 Comparison of Euler and N–S results.

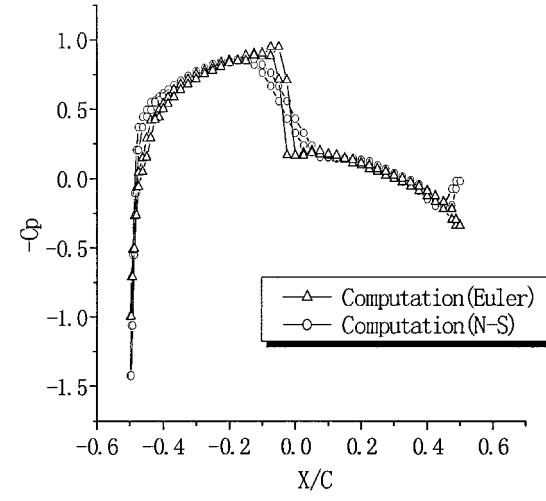

Fig. 5 Distribution of airfoil pressure coefficient for three-dimensional nonrotating wing ($Ma = 0.8$, $\alpha = 0$ deg).

Example Analysis

A O-type body-fitted grid around the sample airfoil (NACA0012) is generated using Thompson's method.[7] The Jameson and Jameson/TVD mixed schemes just described are implemented to solve the Euler equations. Also, the turbulent N–S equations are solved using the Jameson scheme. Grid resolution is Euler: 99×35, N–S: 99×70. As for the N–S calculation, the distance from the airfoil wall to the first layer grid is 2×10^{-5} times of the chord length. An O-H-type grid is generated for the three-dimensional calculation; the grid resolution is for the $99 \times 70 \times 41$ for the nonrotating wing and $99 \times 35 \times 51$ for the rotating wing.

Figure 1 shows the distribution of the surface-pressure coefficient around the sample airfoil for nonzero angle of attack (AOA) and subsonic conditions using the Jameson and TVD/Jameson methods respectively. X represents chordwise position, and the origin of the coordinate system is placed on the midpoint of the airfoil chord. If a shock wave is not present, then the calculation results of these two methods are identical and in good agreement with the results of Ref. 8.

Figure 2 shows the distribution of the surface-pressure coefficient around the sample airfoil (zero AOA and transonic conditions, Jameson and TVD/Jameson methods, respectively). These results are in good agreement with the results of Ref. 9. We can see an apparent pressure leap caused by the shock wave. Also, although the position of the shock wave captured using the TVD method is closer to the leading edge the resolution of the TVD method is higher than the Jameson method. In practice, it takes fewer iteration steps for the TVD scheme to capture the shock wave. However, the iteration time for each step is much longer.

Figure 3 presents the distribution of the surface-friction coefficient around the sample airfoil obtained by solving the N–S equations (Jameson method). The shape of the curve is quite similar to that described in Refs. 10 and 11.

The comparison of the calculation results using Euler and N–S equations is presented in Fig. 4. Because of the viscous effect added in the N–S equations, its shock wave is wider than that acquired by the Euler method. However, the pressure distribution is basically the same. Accordingly, the Euler equations are suitable for lift force calculation. Nevertheless, the N–S equations are necessary for drag force and power calculations of the helicopter rotor.

The distribution of the pressure coefficient for a three-dimensional nonrotating wing ($Ma = 0.8$, $AOA = 0$ deg) is shown in Fig. 5. Figure 6 presents the comparison of the calculation results and experiment data[12] for Caradonna and Tung's rotor blade. Good agreement between them is indicated.

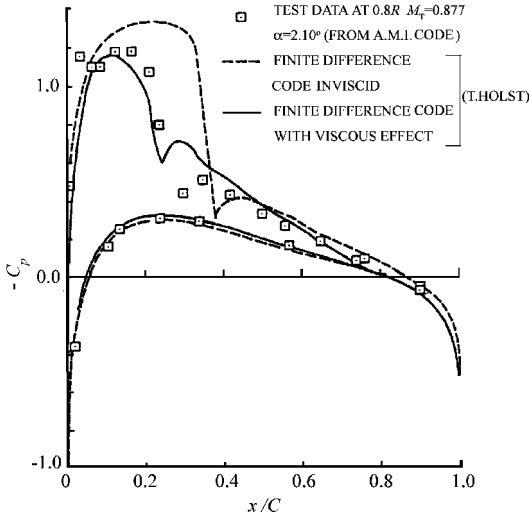

a) Result reported in Ref. 12

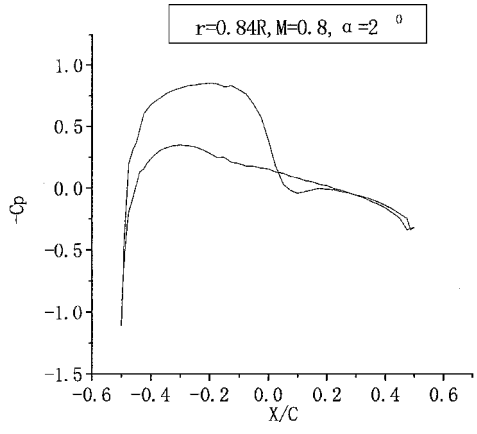

b) Calculation result

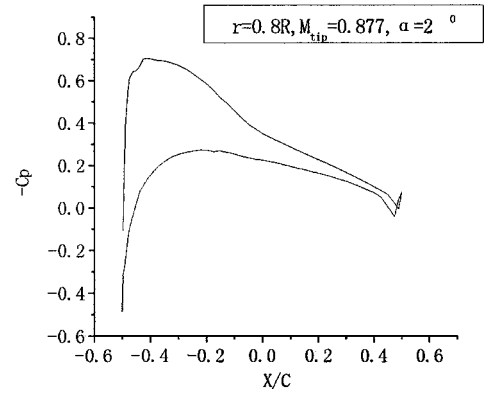

c) Calculation result

Fig. 6 Comparison of the calculation results and experiment data.

References

[1]Davis, S. S., and Chang, I. C., "The Critical Role of Computational Fluid Dynamics in Rotary-Wing Aerodynamics," *Vertica*, Vol. 11, No. 1/2, 1987, pp. 43–63.

[2]Jameson, A., Schmidt, W., and Turkel, E., "Numerical Solution of the Euler Equation by Finite Volume Method Using Runge–Kutta Time-Stepping Schemes," AIAA Paper 81-1259, June 1981.

[3]Yee, H. C., Warming, R. F., and Harten, A., "Implicit Total Variation Diminishing (TVD) Scheme for Steady-State Calculation," AIAA Paper 83-1902, July 1983; also *Journal of Computational Physics*, Vol. 57, No. 3, 1985, pp. 327–360.

[4]Wang, J. C. T., and Widhopf, G. F., "A High-Resolution TVD Finite Volume Scheme for the Euler Equations in Conservation Form," AIAA Paper 87-0538, Jan. 1987.

[5]White, F. M., *Fluid Mechanics*, McGraw–Hill, New York, 1994, pp. 294–446.

[6]Baldwin, B. S., and Lomax, H., "Thin Layer Approximation and Algebraic Model for Separated Turbulent Flows," AIAA Paper 78-257, Jan. 1978.

[7]Thompson, J. F., Thames, F. C., and Mastin, C. W., "Automatic Numerical Generation of Body-Fitted Curvilinear Coordinate System for Fields Containing Any Number of Arbitrary Two-Dimensional Bodies," *Journal of Computational Physics*, Vol. 15, No. 3, 1974, pp. 299–319.

[8]*Handbook of Aerodynamics*, Aeronautical Industry Press, Beijing, 1983 (in Chinese), pp. 3–400.

[9]Deese, J. E., "Numerical Experiment with the Split-Flux-Vector Form of the Euler Equations," AIAA Paper 83-0122, Jan. 1983.

[10]Chakrabartty, S. K., "Numerical Solution of Navier–Stokes Equations for Two-Dimensional Viscous Compressible Flows," *AIAA Journal*, Vol. 27, No. 7, 1989, pp. 843, 844.

[11]Swanson, R. C., and Turkel, E., "A Multistage Time-Stepping Scheme for the Navier–Stokes Equations," AIAA Paper 85-0035, Jan. 1985.

[12]Caradonna, F. X., and Tung, C., "Experimental and Analytical Studies of a Model Helicopter Rotor in Hover," NASA TM-81232, Sept. 1981.